Electronic Supplementary Material (ESI) for Energy & Environmental Science.

Regulating oxygen vacancy and coordination environment of manganese dioxides for enhanced high-mass-loading energy storage

Zhongyou Peng[a], Yuting Huang[a], Alexander G. Bannov[c], Shulong Li[a], Ling Tang[a], Licheng Tan[a]*, Yiwang Chen[a,b]*

Dr. Z. Peng, Y. Huang, Prof. Dr. A. G. Bannov, S. Li, L. Tang, Prof. Dr. L. Tan, Prof. Dr. Y. Chen

[a] College of Chemistry and Chemical Engineering/Institute of Polymers and Energy Chemistry (IPEC)/Film Energy Chemistry for Jiangxi Provincial Key Laboratory (FEC), Nanchang University, 999 Xuefu Avenue, Nanchang 330031, China.

[b] Key Lab of Fluorine and Silicon for Energy Materials and Chemistry of Ministry of Education, Jiangxi Normal University, 99 Ziyang Avenue, Nanchang 330022, China.

[c] Department of Chemistry and Chemical Engineering, Novosibirsk State Technical University, K. Marx 20, Novosibirsk 630073, Russia

*Corresponding Authors: tanlicheng@ncu.edu.cn (L. Tan); ywchen@ncu.edu.cn (Y. Chen).

Experimental Section

***Preparation of High Mass Loading Manganese Oxide (MnO_2) on Carbon Cloth*:**

Electrodeposition of MnO_2 was carried out at 20 mA cm^{-2} on a piece of carbon cloth in a 0.2 M manganese acetate aqueous solution with Ag/AgCl electrode and Pt sheet as the reference and counter electrode, respectively. MnO_2 was electrodeposited at various time of 2, 5, 10, 20, 30 and 40 min to investigate the influence of time on MnO_2 growth, and the as-prepared samples were denoted as MnO_2-2, MnO_2-5, MnO_2-10, MnO_2-20, MnO_2-30, and MnO_2-40, respectively. After electrodeposition, the MnO_2 electrode was washed thoroughly with deionized water and dried at 60 °C under vacuum for 24 h.

***Preparation of Oxygen Vacancy Abundant Manganese Oxide (O_v-MnO_2-30) on Carbon Cloth*:**

The O_v-MnO_2-30 arrays were first synthesized by a facile chemical reduction procedure. Typically, the as-prepared MnO_2-30 was soaked in a 0.5 M aqueous $NaBH_4$ solution at room temperature for 1 h to ensure the complete reaction. After then, the O_v-MnO_2-30 sample was removed from the solution and then dried in vacuum. The mass loadings of O_v-MnO_2-30 is about 12 mg cm^{-2}.

***Assembly of Aqueous ASCs and Quasi-solid-state Planar ASCs*:**

The coin-type cell was comprised by the O_v-MnO_2-30 electrode, activated carbon (AC, YP-50), glass fiber membrane and 1 M Na_2SO_4 aqueous solution as cathode, anode, separator and electrolyte, respectively. A slurry containing the active material of AC, conductive carbon (acetylene black) and binder (PVDF) in a mass ratio of 8: 1: 1 was prepared using N-methyl-2-pyrrolidone (NMP) as a solvent. Next, the obtained slurries were coated on a carbon cloth current collector and then dried at 100 °C for 6 h. For the flexible planar ASCs, the interdigitated electrodes were punched off into fork-shaped patterns using the knife molds. The gel electrolyte (CMC-Na_2SO_4) was prepared by adding 10 g of Na_2SO_4 and 6 g of carboxymethyl cellulose sodium (CMC) into 100 mL of deionized water under quick stirring at 90 °C for 3 h until the gel became transparent. The prepared interdigitated O_v-MnO_2-30 electrode and AC electrode were attached to the side of the flexible PET film, followed by coating with

a thin layer of gel electrolyte. To further enhance the service life, the planar ASCs were further encapsulated by polypropylene tape.

***Assembly of Aqueous O_v-MnO_2-30//Zn Battery*:**

The aqueous O_v-MnO_2-30//Zn Battery was assembled by the O_v-MnO_2-30 electrode, Zn foil, glass fiber membrane and 2 M $ZnSO_4$ + 0.2 M $MnSO_4$ aqueous solution as cathode, anode, separator and electrolyte, respectively.

Material Characterizations

Morphological images were obtained by a field-emission scanning microscopy (SEM, JEOL JSM-6700F) and a field-emission transmission electron microscopy (TEM, JEOL JEM-2100F). Aberration-corrected high-angle annular dark-field scanning TEM (HAADF-STEM) and Electron energy loss spectroscopy (EELS) were obtained with Titan Cubed Themis G2300, JEM-ARM200F. The structure and phase purity of the samples were examined by X-ray diffraction (XRD, PERSEE, XD-3 with Cu Kα radiation, wavelength 0.154 nm), X-ray photoelectron spectroscopy (XPS, Thermo-VG, ESCALAB 250), and Raman spectroscopy (LabRAM HR800). Electron spin resonance (EPR) test was conducted via an EPR spectrometer (JES FA200) at 77 K. The Brunauer–Emmett–Teller surface area was measured using Micromeritics ASAP 2010 surface area and porosity analyzer. The X-ray absorption spectra (XAS) including X-ray absorption near-edge structure (XANES) and extended X-ray absorption fine structure (EXAFS) of the samples were collected at the Singapore Synchrotron Light Source (SSLS) center, where a pair of channel-cut Si (111) crystals was used in the monochromator. The storage ring was working at the energy of 2.5 GeV with average electron current of below 200mA. Kelvin Probe Force Microscopy (KPFM) was employed for potential imaging, which measures the contact potential difference between the probe and sample. Specially, the authors would like to thank Shiyanjia Lab (www.shiyanjia.com) for the KPFM analysis.

In-Situ Electrochemical Raman Spectroscopy

The Raman spectrometer connected with a Teflon electrolysis cell was used to gain Raman spectra. Electrodes were prepared as follows: 10 mg of prepared O_v-MnO_2-30 powder and 50 μL of 5 wt% Nafion perfluorinated resin solution in 950 μL solvent with ethanol and water (v/v, 1:1) were mixed together. Afterwards, the 10 μL ink was coated on surface of glassy carbon electrode. A CV test with a scan rate of 1 mV s^{-1} was also performed to obtain the Raman spectra of the samples.

In-Situ Electrochemical Quartz Crystal Microbalance (EQCM)

The EQCM and CV measurements were performed using a quartz crystal microbalance (EQCM 10M, Gamry) system in combination with an electrochemical workstation (Interface 1010, Gamry). The O_v-MnO_2-30 coated quartz, Pt wire, Ag/AgCl and 1 M Na_2SO_4 were utilized as the working electrode, counter electrode, reference electrode, and electrolyte, respectively. The method of electrode preparation is the same as the above Raman test. The CV test was executed at a sweep rate of 10 mV s^{-1} with coinstantaneous recording resonance frequency. The Sauerbrey equation is utilized to relate mass loading and the resonance frequency variation:

$$\Delta m = -\frac{A\sqrt{\mu_q \rho_q}}{2f_q^2} \cdot \Delta f = -C_f \cdot \Delta f \quad (1)$$

where A is the area of active surface (0.866 cm^2), μ_q is the AT-cut quartz constant (2.947×10^{11} g cm^{-1} s^{-2}), ρ_q is the quartz crystal density (2.65 g cm^{-3}), and f_q is the reference frequency (5.00 MHz), C_f is the sensitivity factor (56.6 ng·cm^{-2}·Hz^{-1} at 20 °C).

The molar weight of intercalated ions can be calculated by Faraday's law:

$$\frac{\Delta m}{\Delta Q} = \frac{M}{nF} \quad (2)$$

where ΔQ is the charge passed through the electrode (C), M is the molar weight of the intercalated ions, F is the Faraday constant (96485 C mol^{-1}), and n is the valence number of the ion.

Computational Details

The Vienna Ab Initio Package (VASP) was employed to perform all the density functional theory (DFT) calculations within the generalized gradient approximation (GGA) using the Perdew-Burke-Enzerhof (PBE) formulation.[1-3] The projected augmented wave (PAW) potentials were applied to describe the ionic cores and take valence electrons into account using a plane wave basis set with a kinetic energy cutoff of 450 eV.[4,5] Partial occupancies of the Kohn–Sham orbitals were allowed using the Gaussian smearing method and a width of 0.05 eV. The electronic energy was considered self-consistent when the energy change was smaller than 10^{-4} eV. A geometry optimization was considered convergent when the force change was smaller than 0.03 eV/Å. Grimme's DFT-D3 methodology was used to describe the dispersion interactions.[6] The equilibrium lattice constants of Si unit cell were optimized when using a 3×3×2 Monkhorst-Pack k-point grid for Brillouin zone sampling. The Climbing Image-Nudged Elastic Band methods had been employed to calculate the Na ions migration barriers in the structures. The adsorption energies (E_{ads}) were calculated as $E_{ads} = E_{ad/sub} - E_{Na} - E_{sub}$, where $E_{ad/sub}$, E_{Na}, and E_{sub} are the total energies of the optimized adsorbate/substrate system, Na atom in the structure, and the clean substrate, respectively.

Electrochemical Measurements:

The CHI 660E workstation was used to perform CV curves, EIS, and GCD curves. The long-term cycling stability was measured by a CT3001A battery tester.

The specific capacitance C (F g^{-1}) and areal capacitance C_A (mF cm^{-2}) of electrodes and devices were calculated from the GCD curves by using the following formula:

$$C = \frac{I\Delta t}{m\Delta V} \text{ or } C_A = \frac{I\Delta t}{A\Delta V} \quad (3)$$

Where I (A) is the discharge current, m (g) is the mass of the active material, and A (cm^{-2}) is the area of the electrode or device, Δt is the discharge time (s) and ΔV is the potential window (V).

The areal energy density E (mWh cm^{-2}) and areal power density P (mW cm^{-2}) of ASCs were defined according to equations:

$$E = \frac{C\Delta V^2}{7200} \tag{4}$$

$$P = \frac{E \times 3600}{\Delta t} \tag{5}$$

The Trasatti analysis method was used to quantify the stored charges (q) at the inner surface (q_i) and outer surface (q_o). The total amount of stored charge (q_T) consists of both q_i and q_o, and the total measured charge q can be further quantified based on the following equations:

$$q_T = q_o + q_i \tag{6}$$

$$q = q_\infty + kv^{-1/2} \tag{7}$$

$$\frac{1}{q} = \frac{1}{q_\infty} + \frac{v^{1/2}}{k} \tag{8}$$

Where $kv^{-1/2}$ and $v^{1/2}/k$ represent the stored charges related to semi-infinite diffusion, k is a constant, and q_∞ is the charge storage at a high scan rate ($v \rightarrow \infty$).

According to the Dunn method, the contribution from diffusion-controlled process and surface reaction can be evaluated by using CV curves.

$$I(V) = k_1 v + k_2 v^{\frac{1}{2}} \tag{9}$$

$$\frac{I(V)}{v^{\frac{1}{2}}} = k_1 v^{\frac{1}{2}} + k_2 \tag{10}$$

Where I is the response current, v is the sweep rate (mV s^{-1}), k_1 and k_2 can be determined from the slope and intercept, respectively. Where $k_1 v$ and $k_2 v^{1/2}$ can be attributed to the surface capacitance contribution and the diffusion-controlled process, respectively.

The real capacitance ($C'(\omega)$) and imaginary capacitance ($C''(\omega)$) from EIS data were calculated by the following equation:

$$C(\omega) = C^{'}(\omega) + jC^{''}(\omega) \quad (11)$$

Where $C'(\omega)$ is the real part of the capacitance $C(\omega)$, $C''(\omega)$ is the imaginary part of the capacitance $C(\omega)$.

The Warburg diffusion coefficient is calculated based on the following equation:

$$D = R^2T^2/2A^2n^4F^4c^2\sigma^2 \quad (12)$$

Where R is the ideal gas constant, T is the absolute temperature, A is the area of electrode, n is electron transfer number, F is the Faraday constant, c is the concentration of Na^+, and σ is the Warburg coefficient.

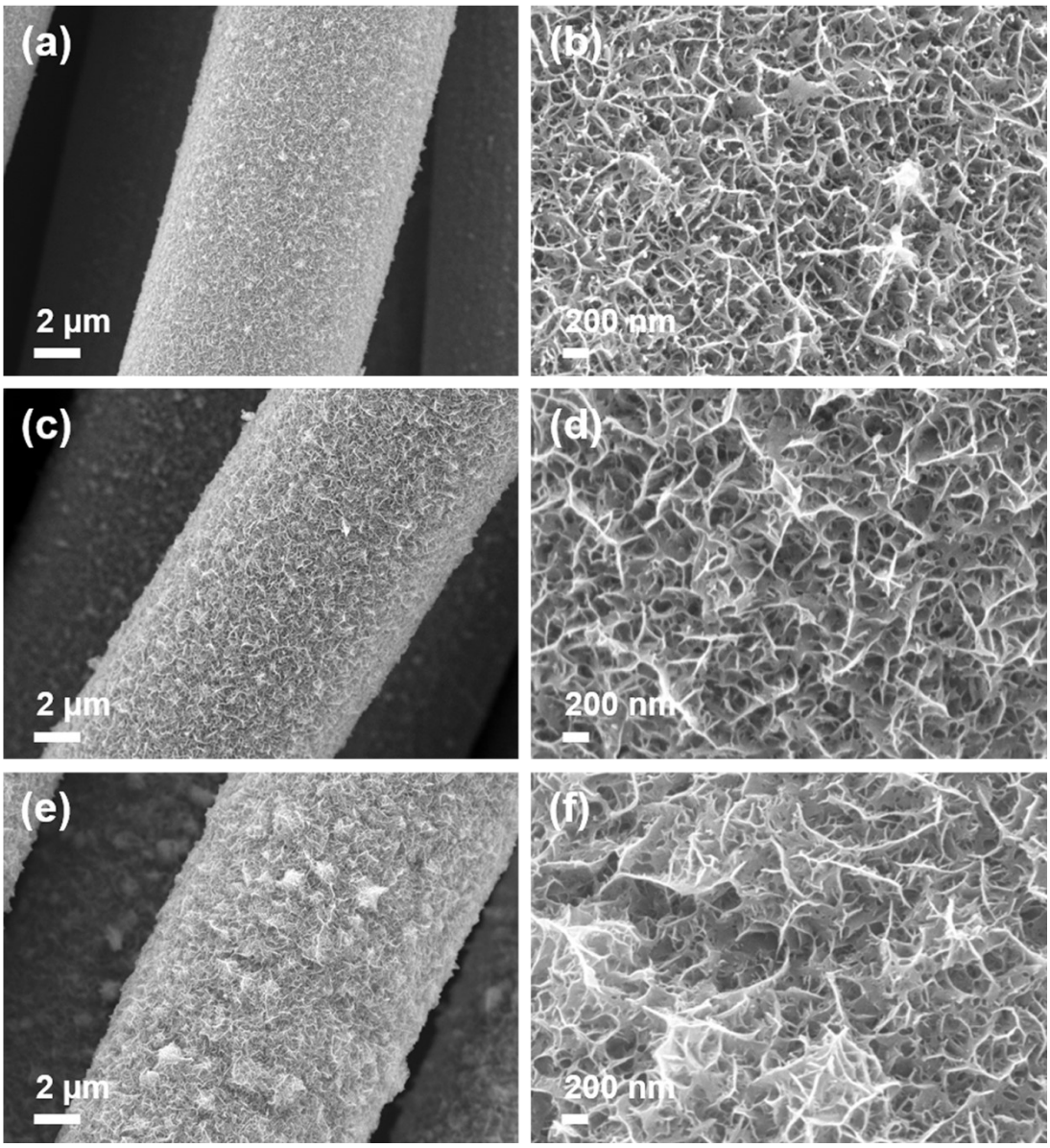

Fig. S1 SEM images of MnO_2 obtained using different electrodeposition times: (a, b) 2 min, (c, d) 5 min, and (e, f) 10 min.

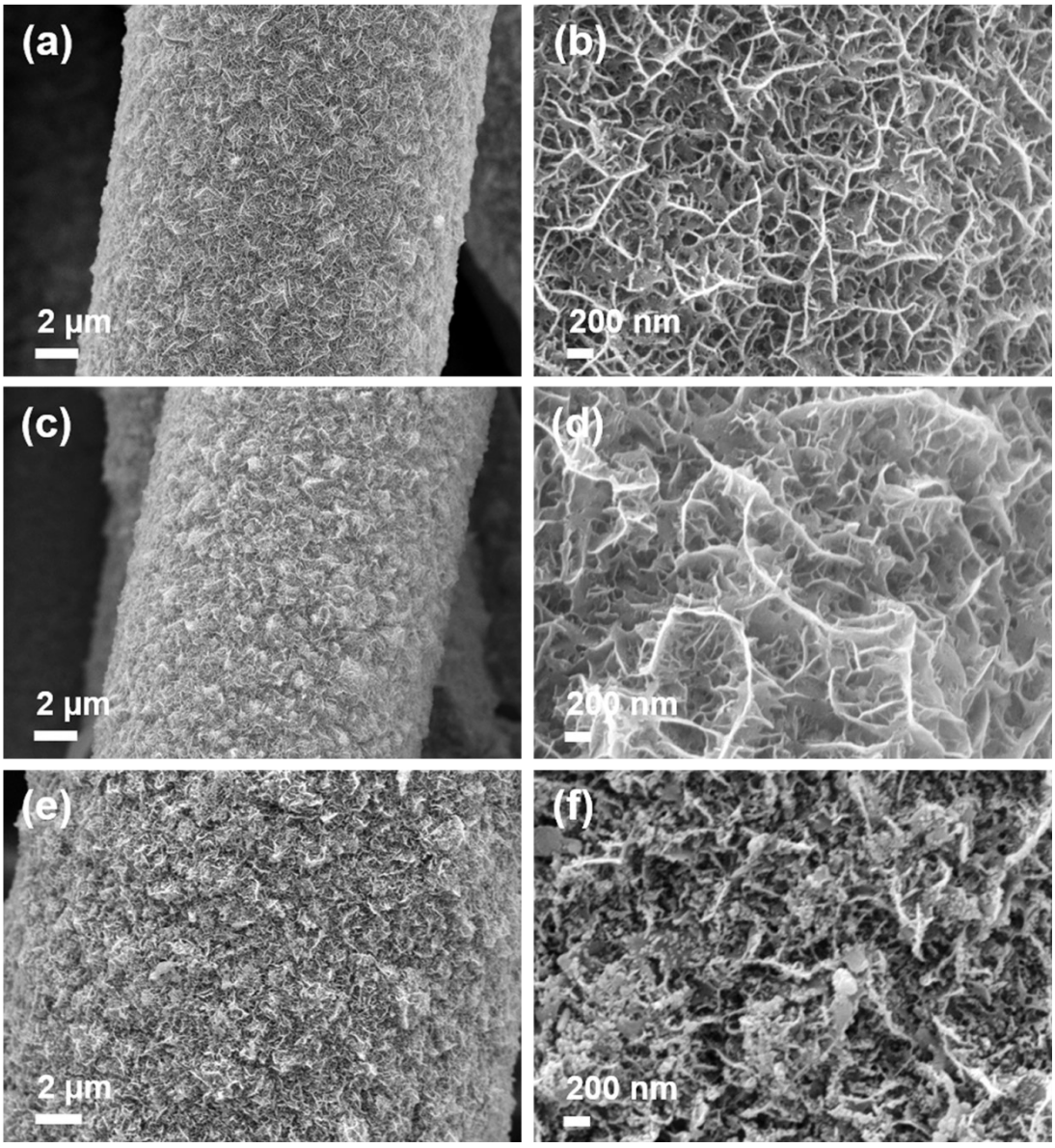

Fig. S2 SEM images of MnO_2 obtained using different electrodeposition times: (a, b) 20 min, (c, d) 30 min, and (e, f) 40 min.

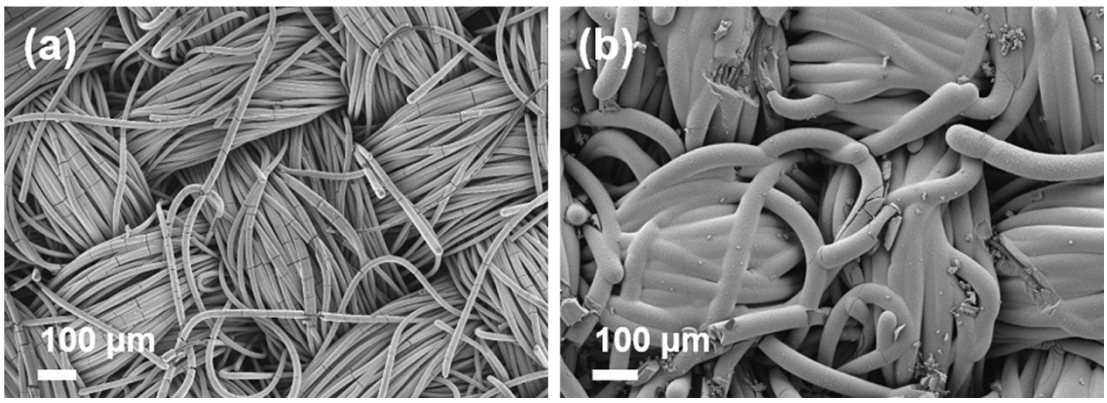

Fig. S3 Low magnification SEM images of MnO_2 electrodes electrodeposited for (a) 30 min and (d) 40 min.

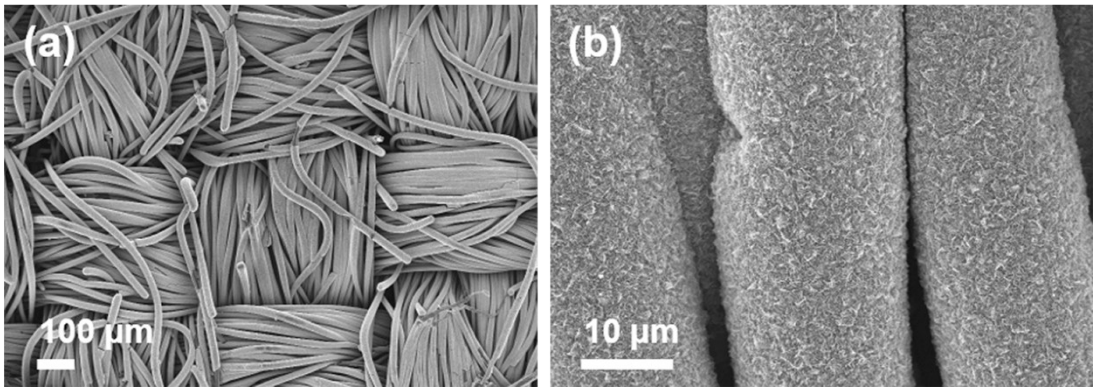

Fig. S4 (a, b) Low magnification SEM images of O_v-MnO_2-30 electrode.

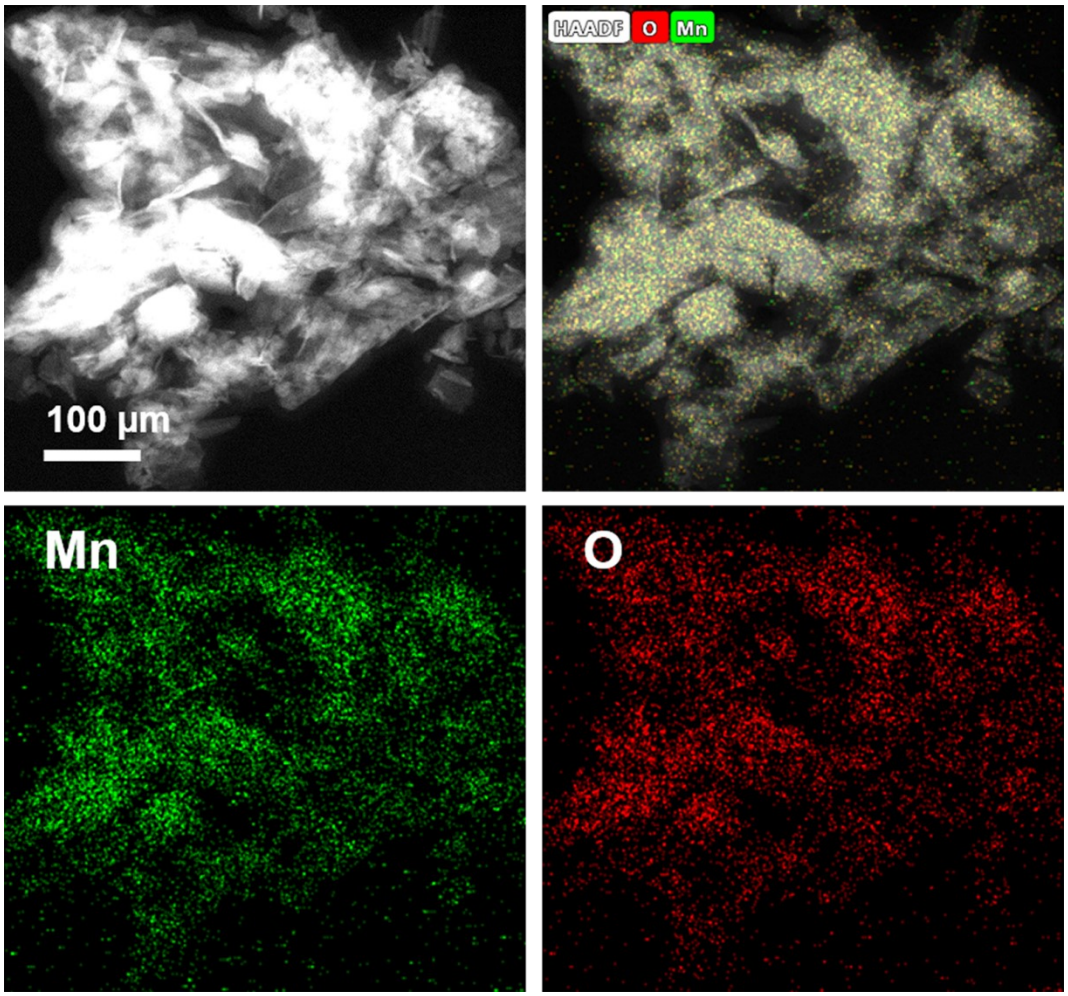

Fig. S5 Element mapping images of O_v-MnO_2-30.

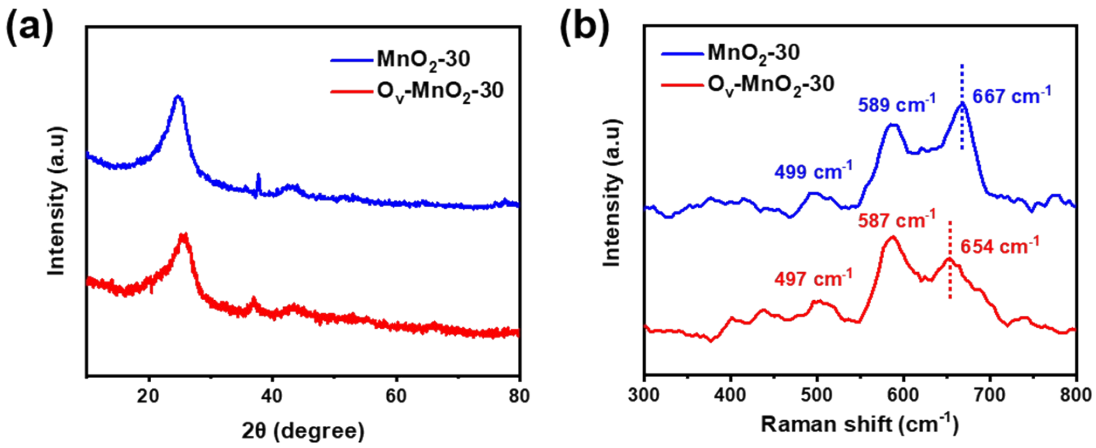

Fig. S6 (a) XRD patterns and (b) Raman spectra of MnO_2-30 and O_v-MnO_2-30 electrodes.

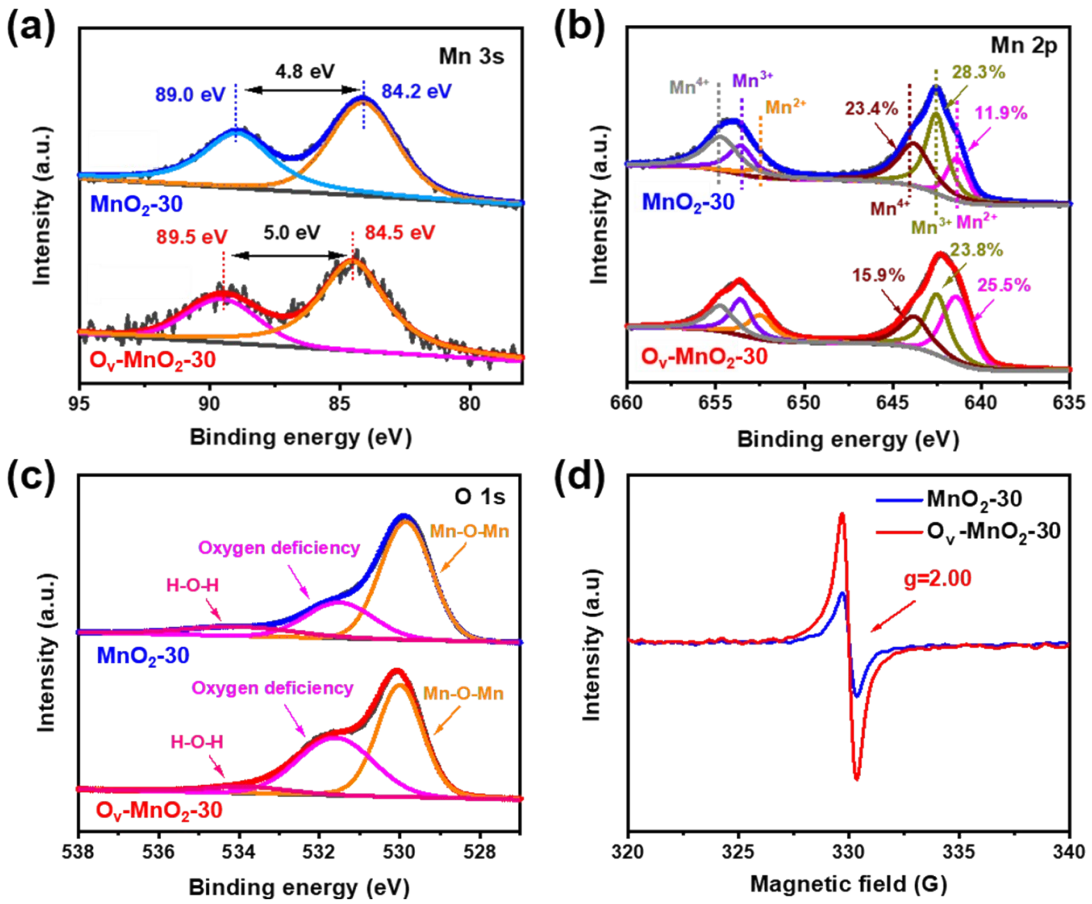

Fig. S7 XPS spectra of MnO_2-30 and O_v-MnO_2-30 electrodes: (a) Mn 3s, (b) Mn 2p, and (c) O 1s. (d) EPR spectra of MnO_2-30 and O_v-MnO_2-30 electrodes.

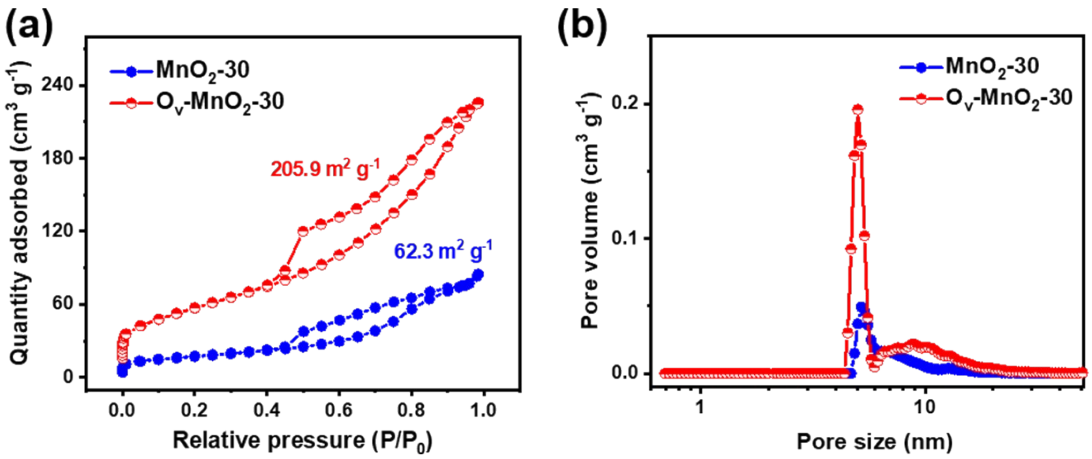

Fig. S8 (a) N_2 adsorption-desorption isotherms of MnO_2-30 and O_v-MnO_2-30. (b) The pore size distribution of MnO_2-30 and O_v-MnO_2-30.

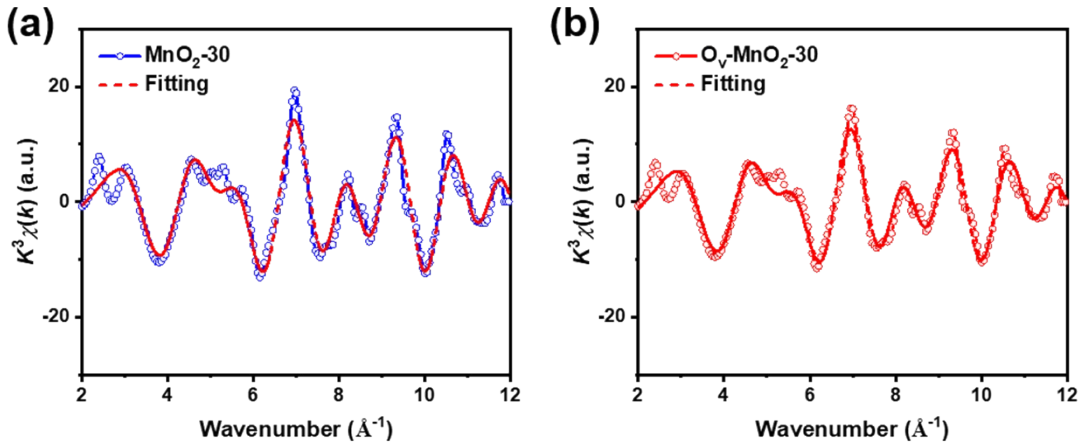

Fig. S9 The EXAFS fitting curve in Magnitude of k^2-weighted Fourier transforms for (a) MnO_2-30 and (b) O_v-MnO_2-30.

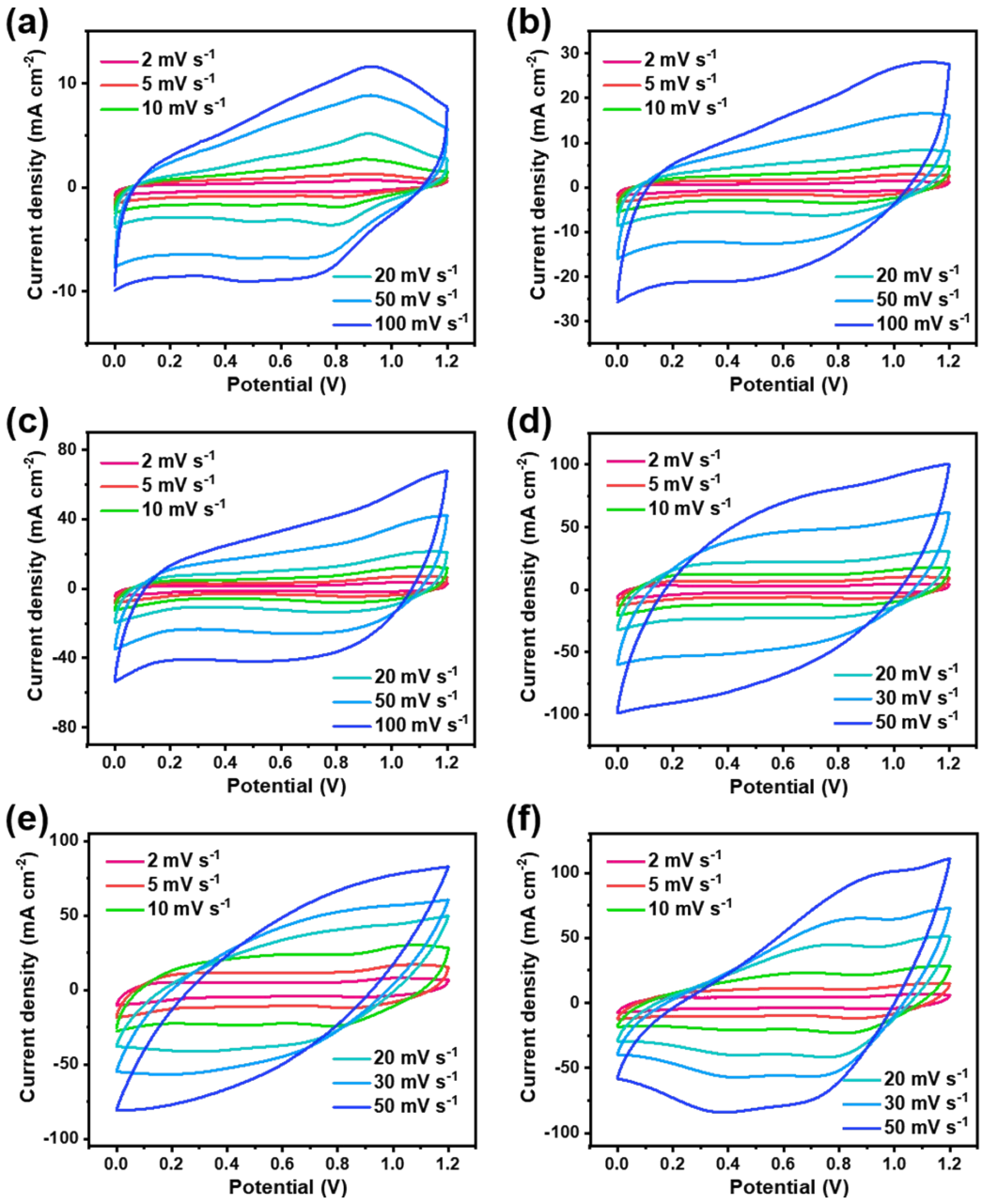

Fig. S10 CV curves of (a) MnO_2-2, (b) MnO_2-5, (c) MnO_2-10, (d) MnO_2-20, (e) MnO_2-30, and (f) MnO_2-40 electrodes collected at different scan rates.

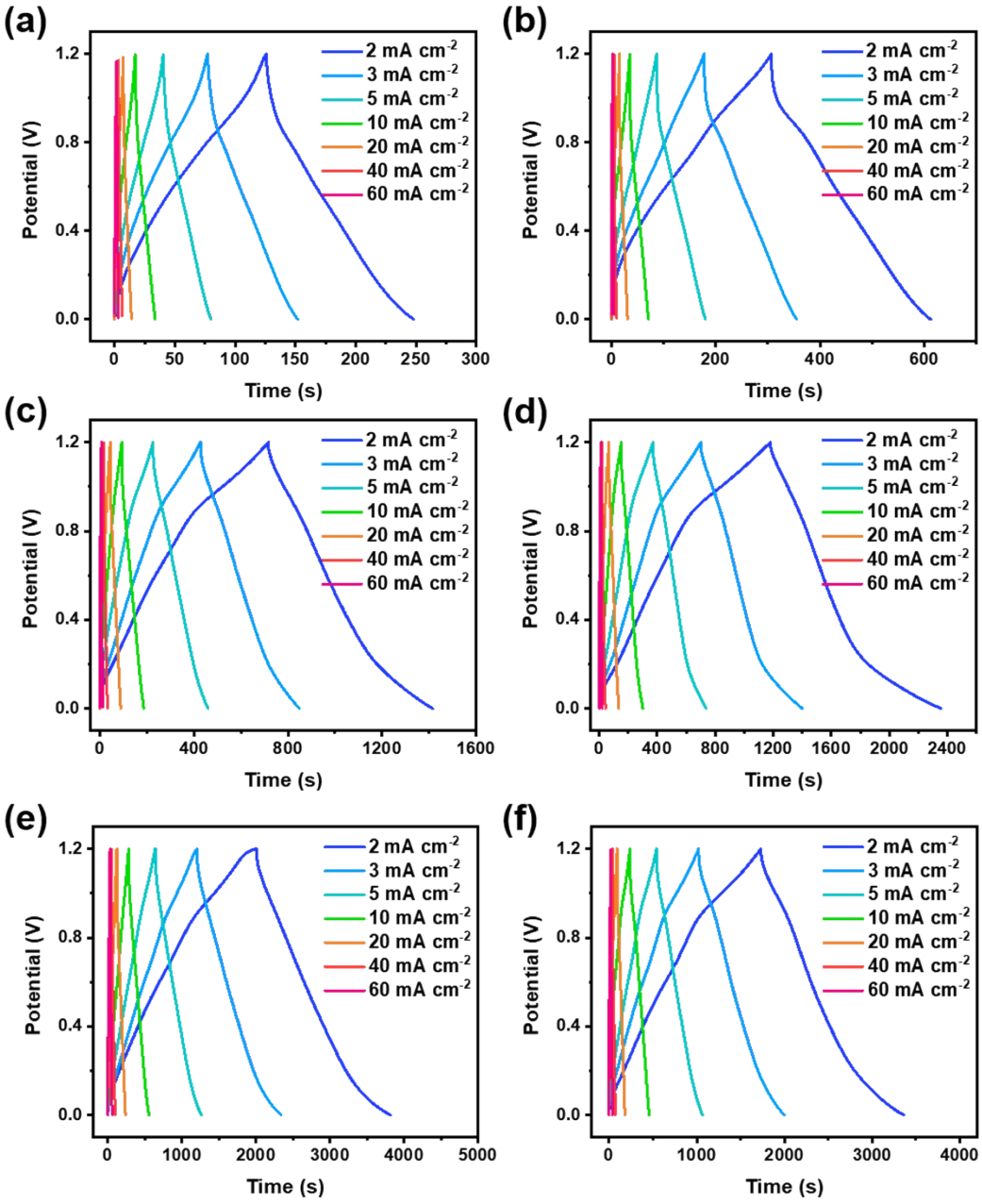

Fig. S11 GCD curves of (a) MnO_2-2, (b) MnO_2-5, (c) MnO_2-10, (d) MnO_2-20, (e) MnO_2-30, and (f) MnO_2-40 electrodes collected at various current densities.

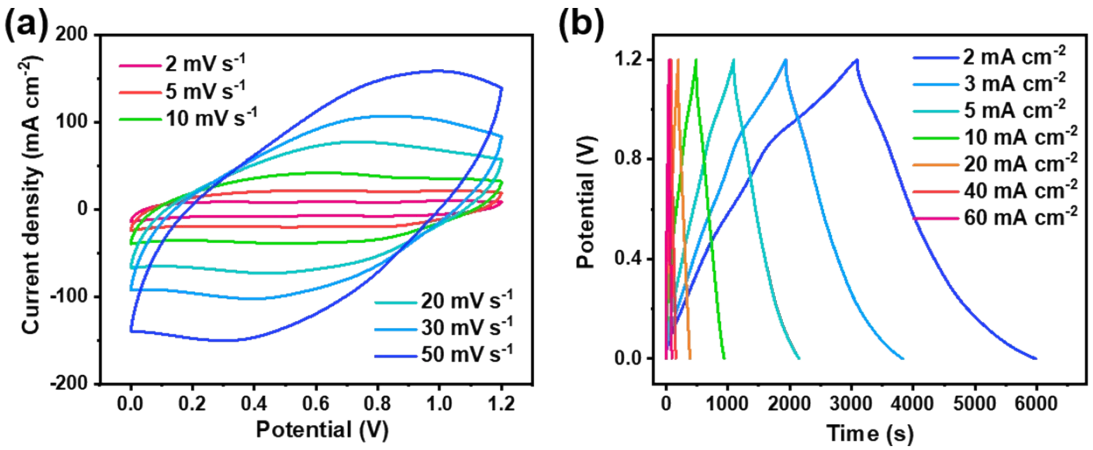

Fig. S12 (a) CV curves of O_v-MnO_2-30 electrode collected at different scan rates. (b) GCD curves of O_v-MnO_2-30 electrode collected at various current densities.

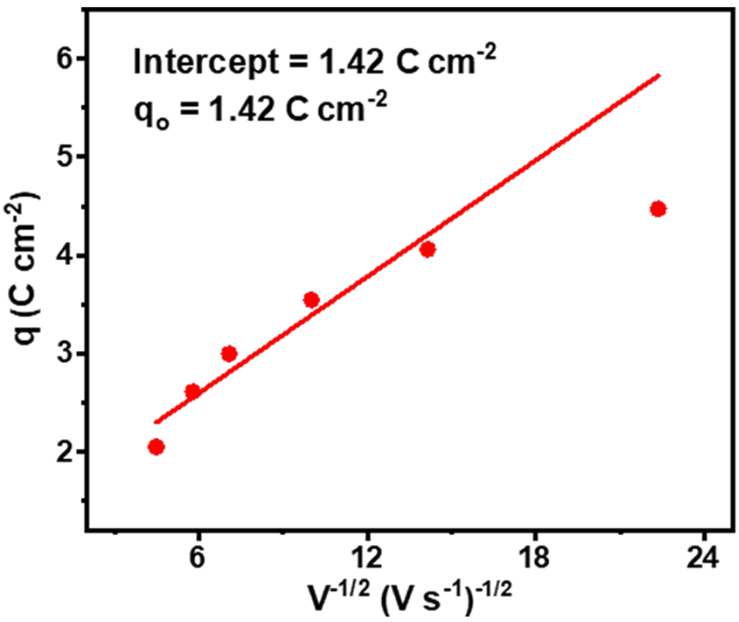

Fig. S13 Stored charge versus inverse of the square root of the scan rate for O_v-MnO_2-30 electrode.

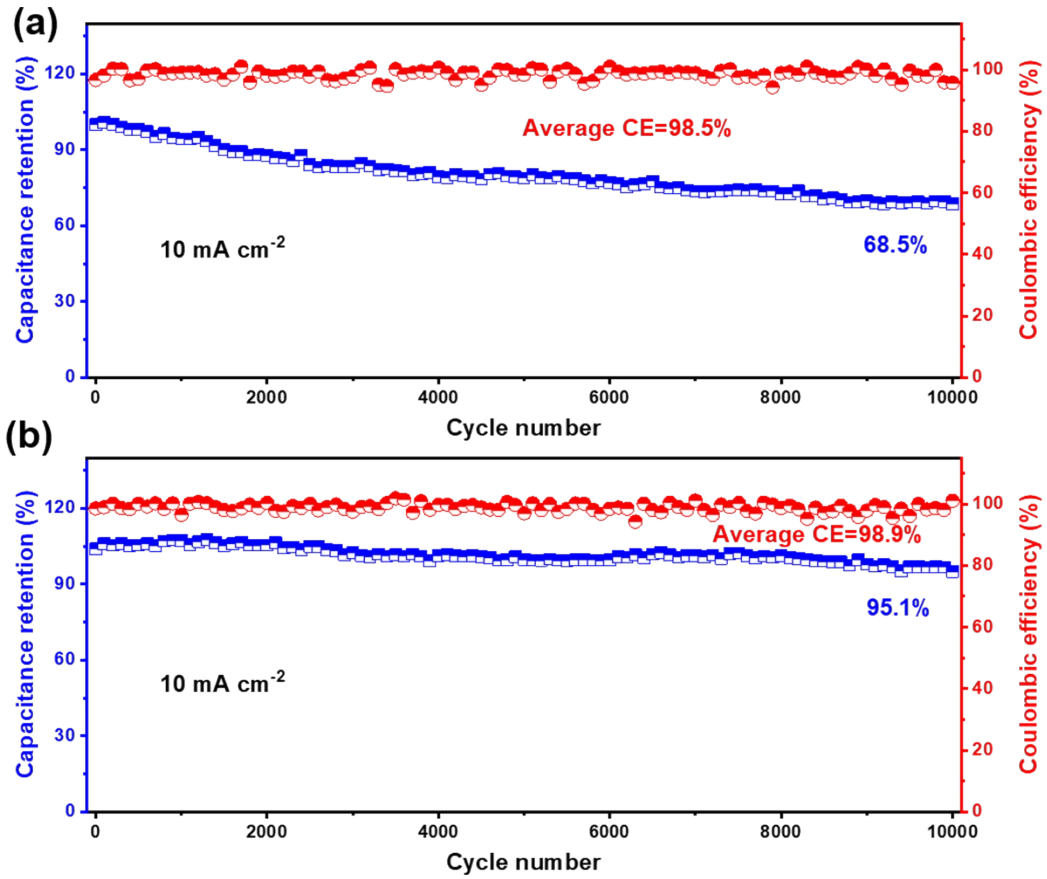

Fig. S14 (a) Cyclic stability and Coulombic efficiency of the (a) MnO_2-30 and (b) O_v-MnO_2-30 electrodes.

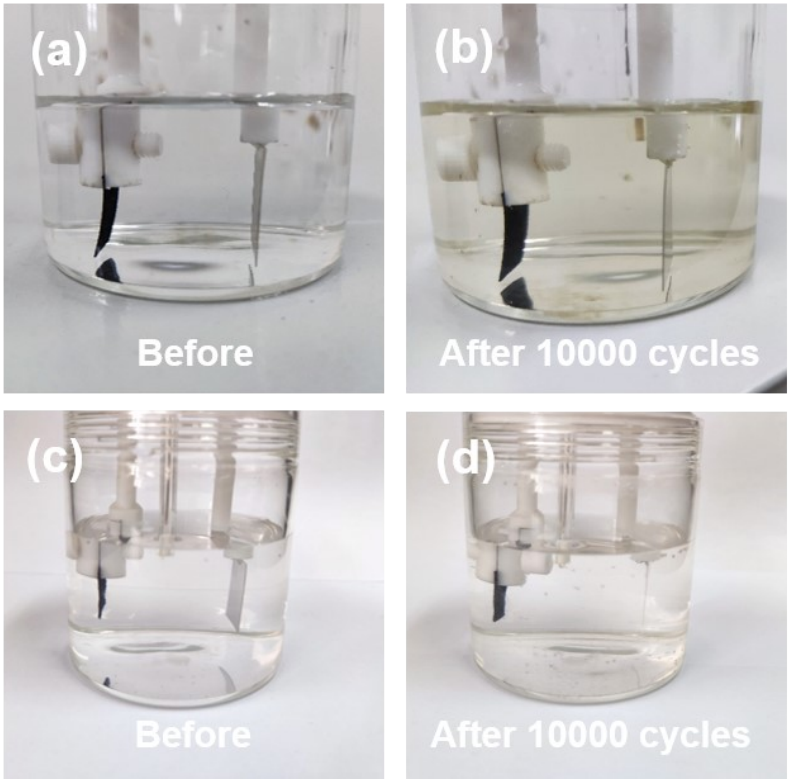

Fig. S15 Digital photographs of electrolytes in (a, b) MnO_2-30 and (c, d) O_v-MnO_2-30 electrodes before and after cycling test.

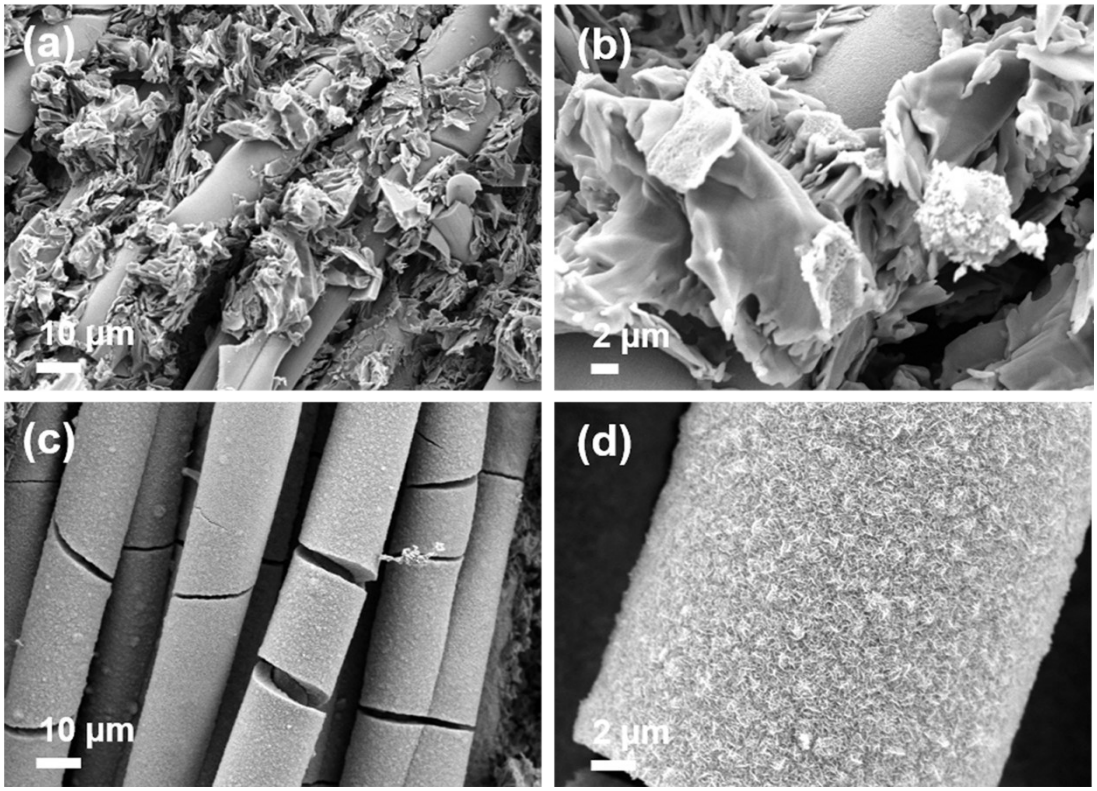

Fig. S16 SEM images of (a, b) MnO_2-30 and (c, d) O_v-MnO_2-30 electrodes after 10 000 cycles at 10 mA cm^{-2}.

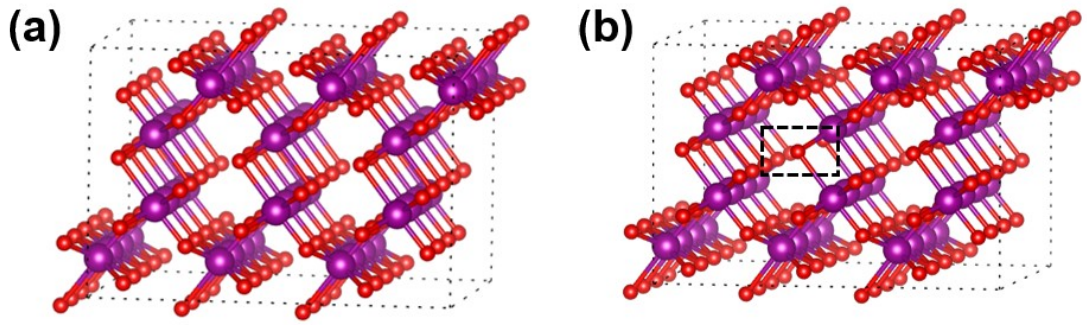

Fig. S17 The optimized structures of (a) MnO_2-30 and (b) O_v-MnO_2-30.

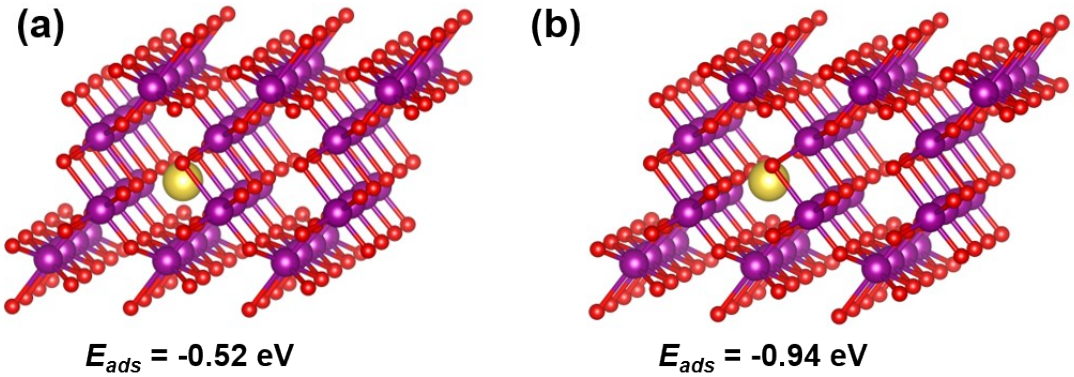

Fig. S18 The adsorption energies of (a) MnO_2-30 and (b) O_v-MnO_2-30 for sodium atoms.

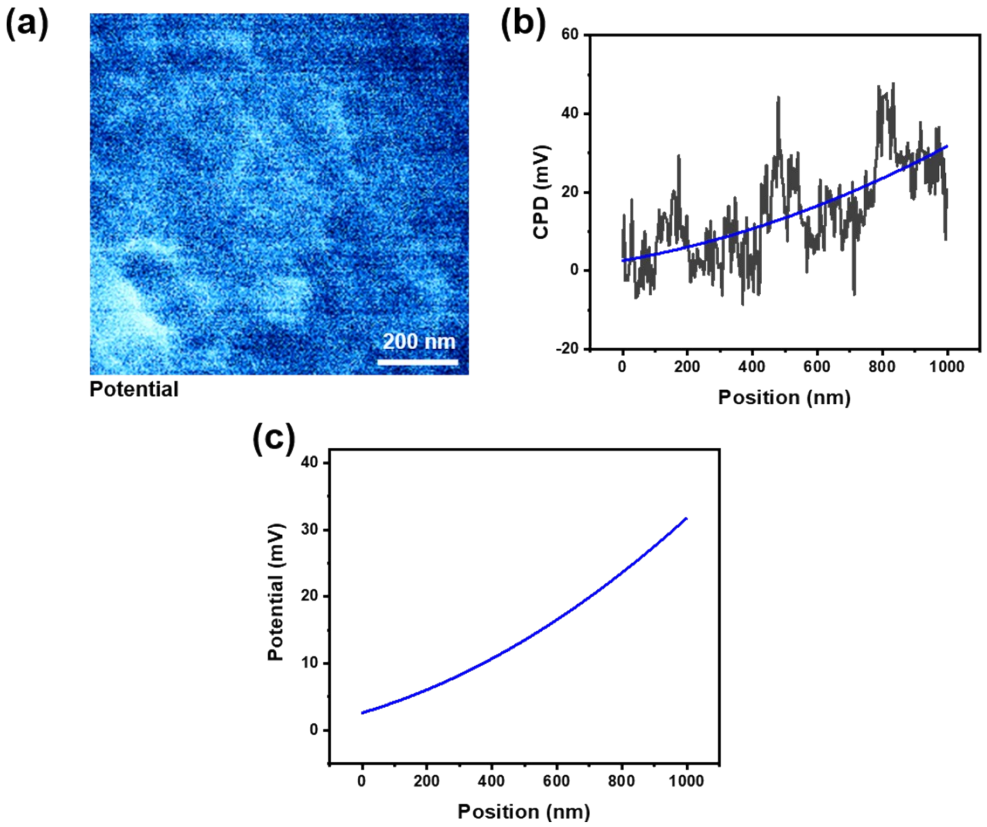

Fig. S19 (a) AFM topographic image, (b) The cross section CPD, (c) The built-in potential distribution of MnO_2-30.

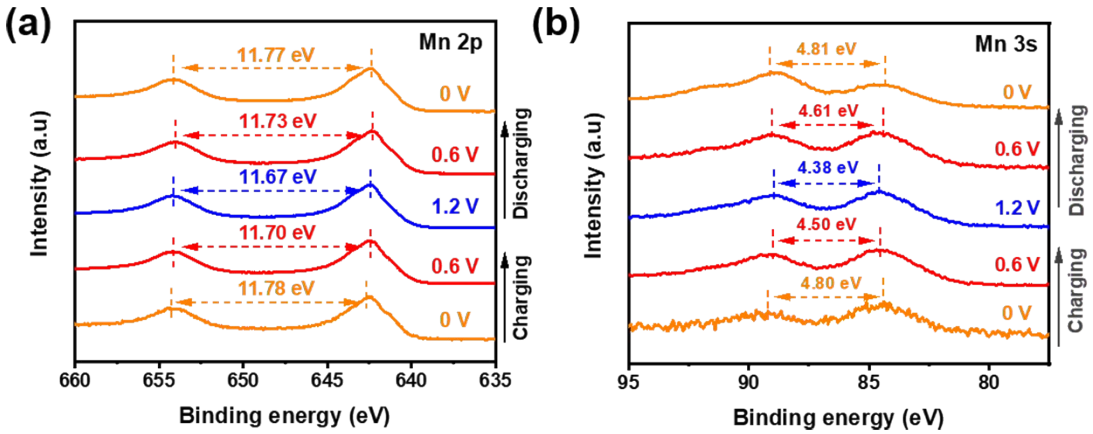

Fig. S20 (a) *Ex-situ* Mn 2p, and (b) *Ex-situ* Mn 3s XPS spectra of O_v-MnO_2-30 electrodes during charging and discharging.

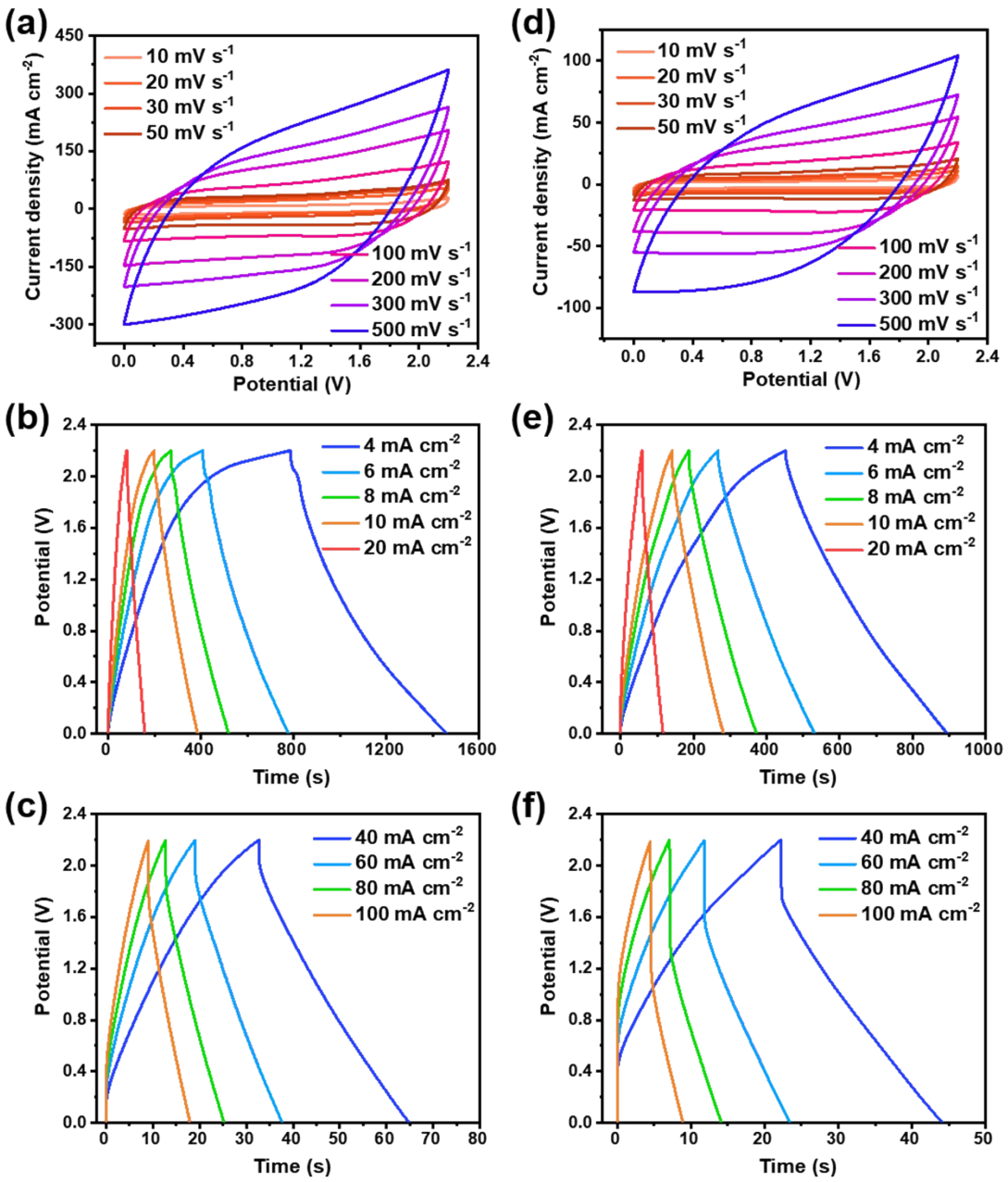

Fig. S21 (a) CV curves and (b, c) GCD curves of the O_v-MnO_2-30//AC ASC. (d) CV curves and (e, f) GCD curves of the MnO_2-30//AC ASC.

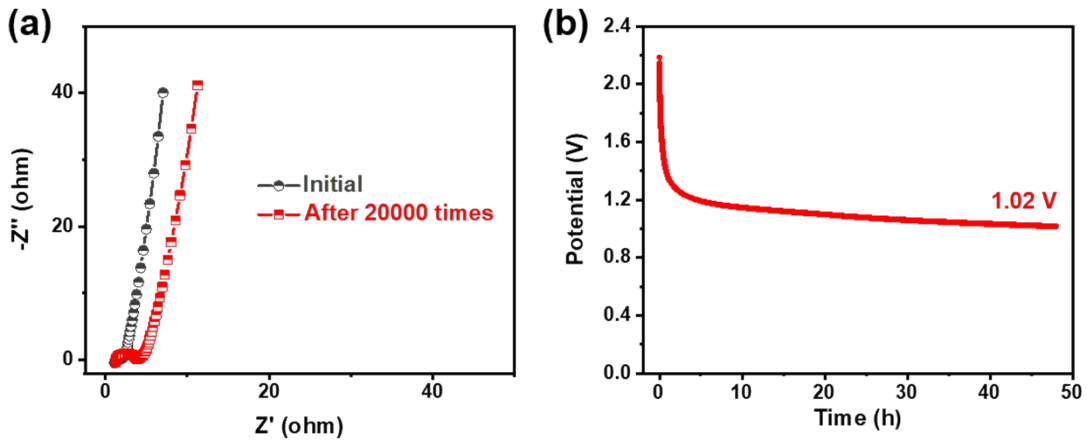

Fig. S22 (a) EIS plots of the O_v-MnO_2-30//AC ASC before and after cycling test. (b) Self-discharge measurement of the O_v-MnO_2-30//AC ASC.

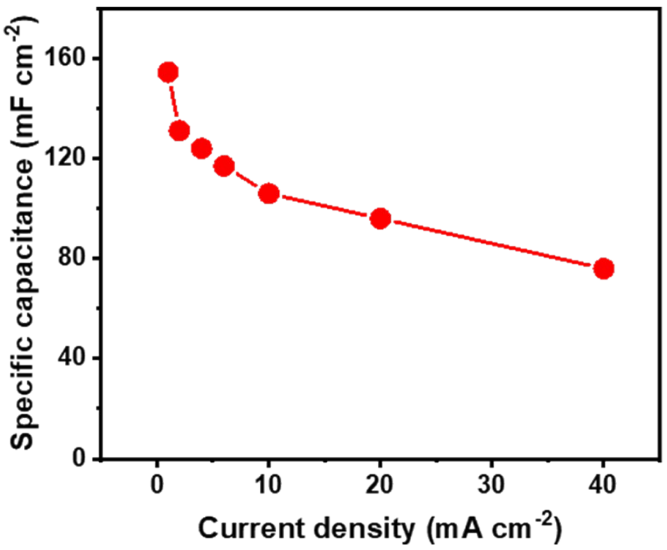

Fig. S23 Areal capacities under different current densities of the O_v-MnO_2-30//AC planar ASC.

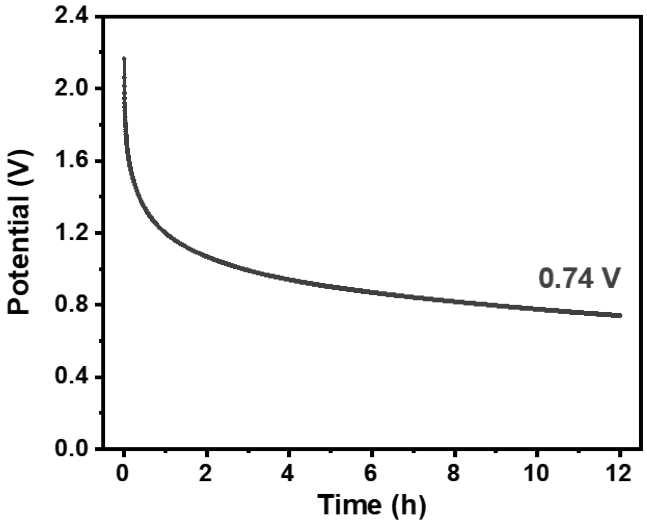

Fig. S24 Self-discharge measurement of the planar ASC.

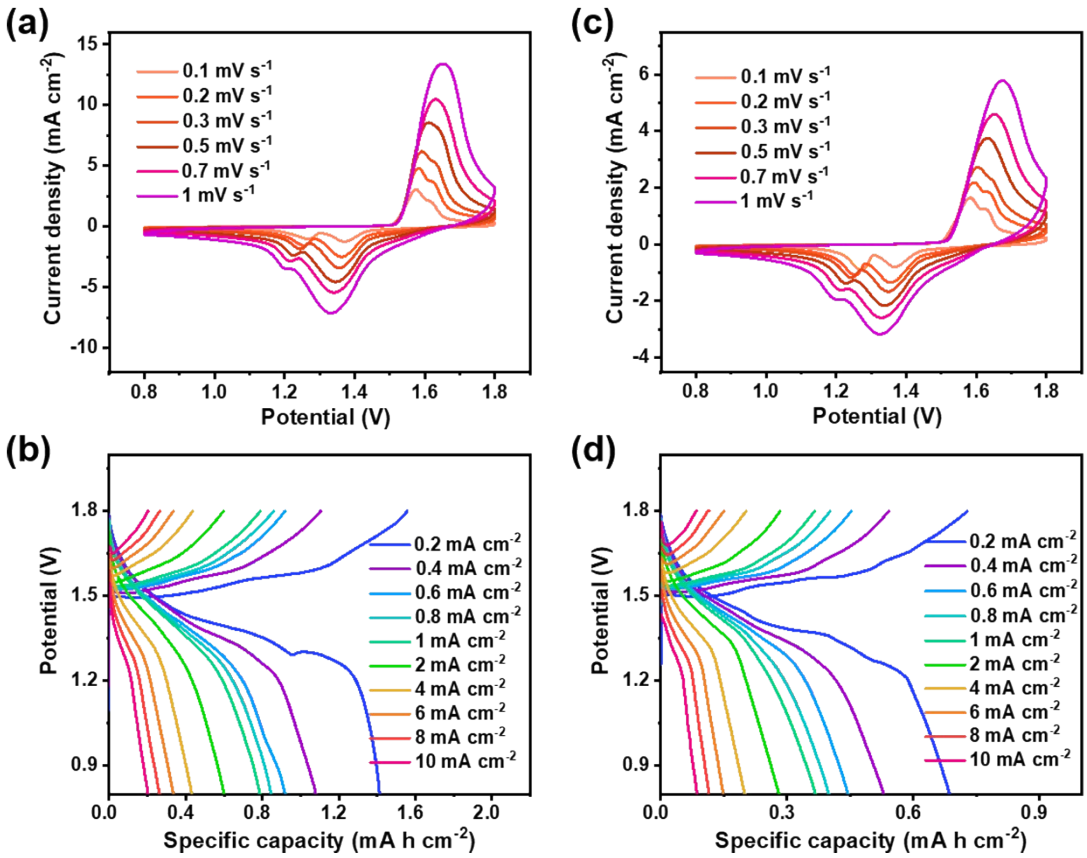

Fig. S25 (a) CV curves, (b) GCD curves of the O_v-MnO_2-30//Zn aqueous battery. (c) CV curves, (d) GCD curves of the MnO_2-30//Zn aqueous battery.

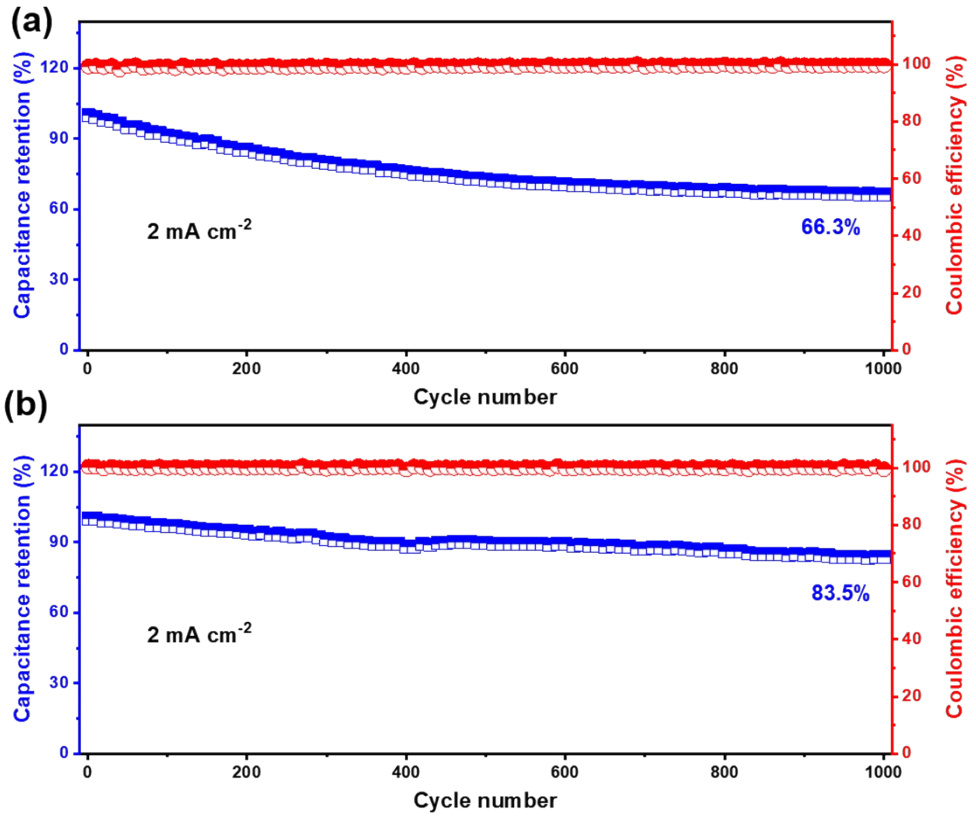

Fig. S26 (a) Cyclic stability and Coulombic efficiency of the (a) MnO_2-30//Zn ZIB and (b) O_v-MnO_2-30//Zn ZIB.

Table S1. Analysis and further fitting results of EXAFS data.

Sample	Shell	*CN*	*R* (Å)	σ^2 (Å^2)	ΔE_0 (eV)	*R* factor
Mn foil	Mn-Mn	4*	2.64±0.01	0.0073	4.2	0.0139
MnO_2-sample	Mn-O	6.0±0.4	1.88±0.01	0.0027	11.9	0.0157
	Mn-Mn1	3.0±1.4	2.87±0.01	0.0046	9.5	
	Mn-Mn2	5.2±1.6	3.42±0.01	0.0015	9.4	
MnO_2-30	Mn-O	6.1±0.8	1.89±0.01	0.0033	10.6	0.0152
	Mn-Mn	5.1±0.9	2.87±0.01	0.0027	9.5	
O_v-MnO_2-30	Mn-O	5.6±0.6	1.90±0.01	0.0035	11.8	0.0122
	Mn-Mn	4.6±0.8	2.88±0.01	0.0033	10.4	

CN, coordination number; *R*, distance between absorber and backscatter atoms; σ^2, Debye-Waller factor to account for both thermal and structural disorders; ΔE_0, inner potential correction; *R* factor indicates the goodness of the fit. S_0^2 was fixed to 0.719, according to the experimental EXAFS fit of Mn foil by fixing CN as the known crystallographic value. A reasonable range of EXAFS fitting parameters: $0.600 < S_0^2 < 1.000$; $CN > 0$; $\sigma^2 > 0$ Å^2; $|\Delta E_0| < 15$ eV; *R* factor < 0.02.

Table S2. The kinetic parameters of MnO_2-30 and O_v-MnO_2-30 electrodes. R_s: Ohmic resistance (Ω); R_{ct}: Charge transfer resistance (Ω); σ: The slope of the plot of Z (Ω $Hz^{1/2}$); D_{Na}: Sodium diffusion coefficient ($cm^2\ s^{-1}$).

Samples	R_s	R_{ct}	σ	D_{Na}
MnO_2-30	5.12	0.91	3.59	6.83×10^{-10}
O_v-MnO_2-30	3.63	0.37	1.05	7.98×10^{-9}

Table S3. Electrochemical properties for O_v-MnO_2 electrode in comparison with those Mn-based electrode materials in earlier reports.

Electrodes	Method	Electrolytes	*C* ($F\ g^{-1}$)	*C* ($mF\ cm^{-2}$)	Rate capability	*Ref.*
Al-Doped MnO_2	HT	0.5 M Na_2SO_4	213 at 0.1 A g^{-1}	852 at 0.1 A g^{-1}	51.5% [0.1-5 A g^{-1}]	7
α-MnO_2/*β*-MnO_2	HT	1 M LiCl	233 at 1 mV s^{-1}	783 at 1 mV s^{-1}	50.0% [1-20 mV s^{-1}]	8
$Ni_{0.25}Mn_{0.75}O$@C	HT+CN	1 M LiCl	-	242.9 at 1 mA cm^{-2}	24.9% [1-16 mA cm^{-2}]	9
β-MnO_2@d-MnO_2	HT+RD	1 M Na_2SO_4	657	788	58.8% [0.25-32 A g^{-1}]	10
Heter-MnO_2-1.38	HT+RD	1 M Na_2SO_4	-	4762 at 1 mA cm^{-2}	79% [1-100 mA cm^{-2}]	11
WC@MnO_2	RD	6 M KOH	87 at 1 mA cm^{-2}	3620 at 1 mA cm^{-2}	43.0% [1-20 mA cm^{-2}]	12
CNT/MnO_2-25/GCC	RD	1 M Na_2SO_4	371.4 at 1 mA cm^{-2}	3380 at 1 mA cm^{-2}	53.3% [1-30 mA cm^{-2}]	13
CNT/MnO_2-25/ECC	RD	1 M Na_2SO_4	-	1660 at 1 mA cm^{-2}	48.0% [1-30 mA cm^{-2}]	13
MnO_2 Nanosheets	RD	0.5 M Na_2SO_4	1035 at 2 mV s^{-1}	91.7 at 2 mV s^{-1}	24.6% [2-100 mV s^{-1}]	14
MnO_2/TCC	RD	5 M LiCl	464 at 4 mA cm^{-2}	2088 at 4 mA cm^{-2}	-	15
MnO_2@CNTs @3DGA-7.5	CVD	1 M Na_2SO_4	200 at 5 mV s^{-1}	1500 at 5 mV s^{-1}	42.7% [5-100 mV s^{-1}]	16
MnO_2@WC	ED	1 M Na_2SO_4	118.7 at 1 mA cm^{-2}	3204 at 1 mA cm^{-2}	87.4% [1-30 mA cm^{-2}]	17
α-MnO_2 Nanoflowers	EP	6 M KOH	630	315	-	18
MnO_2-60	ED	1 M Na_2SO_4	332 at 1 mA cm^{-2}	3320 at 1 mA cm^{-2}	57.2% [1-30 mA cm^{-2}]	19
MnO_2 Nanosheets	ED	1 M Na_2SO_4	640 at 1 mA cm^{-2}	1472 at 1 mA cm^{-2}	23.4% [1-10 mA cm^{-2}]	20
NNA@MnO_2	ED	0.5 M Na_2SO_4	214 at 1 mV s^{-1}	749 at 1 mV s^{-1}	-	21
MnO_2 Nanoflower	ED	1 M Na_2SO_4	110 at 3 mA cm^{-2}	525 at 3 mA cm^{-2}	54.0% [3-20 mA cm^{-2}]	22
$NaMnO_2$	ED	1 M Na_2SO_4	328 at 5 mV s^{-1}	1000 at 5 mV s^{-1}	33.3% [5-200 mV s^{-1}]	23
O-deficient MnO_2 Nanorods	ED	0.5 M Na_2SO_4	306 at 10 mV s^{-1}	153 at 10 mV s^{-1}	53.5% [10-100 mV s^{-1}]	24
MnO_x-h Nanosheet	ED	5 M LiCl	173.3 at 5 mV s^{-1}	1300 at 5 mV s^{-1}	57.7% [5-100 mV s^{-1}]	25
MnO_2-30	**ED+CR**	**1 M Na_2SO_4**	**252.5 at 2 mA cm^{-2}**	**3030.1 at 2 mA cm^{-2}**	**41.2% [2-60 mA cm^{-2}]**	**This work**
O_v-MnO_2-30	**ED+CR**	**1 M Na_2SO_4**	**402.6 at 2 mA cm^{-2}**	**4831.6 at 2 mA cm^{-2}**	**46.3% [2-60 mA cm^{-2}]**	**This work**

Notes: CVD: Chemical vapor deposition; ED: Electrodeposition; EP: Electrospinning; RD: Redox deposition; HT: Hydrothermal reaction; TD: Thermal decomposition; CN: Calcination; Chemical reduction (CR)

Table S4. Comparison of O_v-MnO_2//AC ASC with some state-of-the-art SCs reported in the literature.

Devices	Voltage (V)	C (F cm^{-2})	E_{areal} (mW h cm^{-2})	P_{areal} (mW cm^{-2})	*Ref.*
SHS@SC	1.6	2.91	1.05	-	26
MnO//V_2O_5	2	1.49	0.83	-	19
MnO_2/CNF//Bi_2O_3/CNF	1.8	0.09	0.04	12.9	22
FEG/MoO_{3-x}//FEG	2	0.99	0.55	-	27
AC/CNT/GO//AC/CNT/GO	1	4.54	0.63	-	28
$Mo_{0.1}W_{0.9}O_{3-x}$ SS/SWCNTs//AC	2	0.23	0.11	22	29
VO_x/rGO//G-VNQDs/rGO	1.6	0.21	0.09	4	30
Ni-Mn-O//AC	2.4	0.15	0.08	13	9
MNCFT//ONCFT	1.6	0.78	0.28	26.5	31
rGO/CNT//NiCoBOH	1.4	0.08	0.078	16.3	32
MnO_2//AC	**2.2**	**0.80**	**0.54**	**110**	**This work**
O_v-MnO_2//AC	**2.2**	**1.23**	**0.83**	**110**	**This work**

Table S5. Comparison of electrochemical performance of the state-of-the-art planar SCs prepared by different printing technologies.

Devices	Interdigital electrode fabrication	Voltage (V)	E_{areal} (μW h cm^{-2})	P_{areal} (mW cm^{-2})	*Ref.*
LIG-FeOOH//LIG-MnO_2	Laser scribing	1.8	9.6	11.8	33
AC//MnO_2	Laser scribing	1.5	10	-	34
VN NSAs//$NaMnO_x$@NCF	Laser scribing	2.4	87.62	12.1	35
PPy-MWCNT//MnO_2@PPy	Laser scribing Electrodeposition	1.6	12.16	17.6	36
LIG/Fe_3O_4//LIG	Laser scribing	1.0	60.2	0.75	37
CNT//PANI	Laser scribing	2.3	48.6	5.4	38
rGO	Laser scribing	0.8	0.51	2.4	39
Ni-CAT MOF/LSG	Laser scribing	1.4	4.1	7	40
LIG-N-PEDOT	Laser scribing	0.8	64	32.9	41
FeHCF-graphene//CuHCF-graphene	Vacuum filtration	1.8	9	-	42
VN//MnO_2	Vacuum filtration	2.0	9	0.6	43
Ni_2[CuPc$(NH)_8$]/EG	Vacuum filtration	0.8	1.7	168	44
graphene/CNT/PH1000	Vacuum filtration	0.8	1.27	1.22	45
Zn//AC	Electrodeposition	1.5	115.4	3.9	46
VN//P-TiON	Electrodeposition	1.8	32.4	45	47
V_2O_5-CNT//MnO_2-CNT	Electrodeposition	1.6	0.88	0.63	48
PPy//MnO_2	Electrodeposition	1.5	8.05	7.32	49
NiCoP@NiOOH//ZIF-C	Electrodeposition	1.4	13.9	2	50
CNT//Zn	Electrodeposition	1.8	28	7.8	51
MoS_2	Direct ink writing	2.0	89.2	-	52
MXene	3D printing	0.6	100	19.7	53
MXene-AgNW-MnONW-C60	3D printing	0.8	19.2	58.3	54
MXene	3D printing	0.6	24.4	6	55
$Ti_3C_2T_x$//CoAl LDH	Screen-printing	1.45	8.8	0.77	56
RGO-PE//GO/PAPE	Screen-printing	1.2	4.83	25.3	57
$Ti_3C_2T_x$	Stamp-printing	0.6	0.76	0.33	58
graphene	Stamp-printing	1.4	5.9	6	59
$Cu(OH)_2$@FeOOH/Cu	Solution-immersion	1.5	18.1	0.73	60
Be^{2+}-MXene	Solution-immersion	0.6	3.86	-	61
3DGN/SWNT/AgNW	Spray coating	1	2.75	0.36	62
$Ti_3C_2T_x$	Inkjet printing	0.5	0.32	0.158	63
$Ti_3C_2T_x$/CuFe-PBA	Inkjet printing	1.6	70.5	52	64
G-CNT	Inkjet printing	1.0	1.36	0.25	65
MoS_2/rGO	Inkjet printing	1.75	3.85	12.6	66
O_v-MnO_2//AC	**Cut-and-transfer**	**2.2**	**103.9**	**44**	**This work**

Table S6. Comparison of O_v-MnO_2-30//Zn device with some state-of-the-art zinc ion batteries reported in the literature.

Electrode	Electrolyte	Capacity (mA h cm^{-2})	*Ref.*
MnO_2@PEDOT//Zn	1 M $Zn(NO_3)_2$ + 0.1 M $MnSO_4$	1.02 at 2 mA cm^{-2}	67
CNTs@MnO_2//Zn-CNTs	2 M $ZnSO_4$ + 0.2 M $MnSO_4$	0.96 at 1 mA cm^{-2}	68
Zn-δ-NMOH//Zn/CC	2 M $ZnCl_2$ + 0.2 M $MnSO_4$	1.43 at 1 mA cm^{-2}	69
N-CNSs@MnO_2//NCNSs@Zn	2 M $ZnSO_4$ + 0.2 M $MnSO_4$	0.698 at 0.46 mA cm^{-2}	70
MnO_2/Zn	2 M $ZnSO_4$ + 0.1 M $MnSO_4$	1.1 at 1.5 mA cm^{-2}	71
Na:MnO_2/GCF//Zn/GCF	2 M $ZnSO_4$ + 0.1 M $MnSO_4$	0.573 at 0.15 mA cm^{-2}	72
Zn_xMnO_2//ACC/Zn	2 M $ZnSO_4$ + 0.4 M $MnSO_4$	0.97 at 2 mA cm^{-2}	73
MnO_2-30//Zn	**2 M $ZnSO_4$ + 0.2 M $MnSO_4$**	**0.68 at 0.2 mA cm^{-2}**	**This work**
O_v-MnO_2-30//Zn	**2 M $ZnSO_4$ + 0.2 M $MnSO_4$**	**1.41 at 0.2 mA cm^{-2}**	**This work**

References

1 G. Kresse and J. Furthmüller, *Phys. Rev. B*, 1996, **54**, 11169-11186.

2 J. P. Perdew, K. Burke and M. Ernzerhof, *Phys. Rev. Lett.*, 1996, **77**, 3865.

3 G. Kresse and D. Joubert, *Phys. Rev. B*, 1999, **59**, 1758.

4 P. E. Blöchl, *Phys. Rev. B*, 1994, **50**, 17953-17979.

5 S. Grimme, J. Antony, S. Ehrlich and H. Krieg, *J. Chem. Phys.*, 2010, **132**, 154104.

6 G. Henkelman, B. P. Uberuaga and H. Jónsson, *J. Chem. Phys*., 2000, **113**, 9901-9904.

7 Z. Hu, X. Xiao, C. Chen, T. Li, L. Huang, C. Zhang, J. Su, L. Miao, J. Jiang, Y. Zhang and J. Zhou, *Nano Energy*, 2015, **11**, 226-234.

8 C. Zhu, L. Yang, J. K. Seo, X. Zhang, S. Wang, J. Shin, D. Chao, H. Zhang, Y. S. Meng and H. J. Fan, *Mater. Horiz.*, 2017, **4**, 415-422.

9 W. Zuo, C. Xie, P. Xu, Y. Li and J. Liu, *Adv. Mater.*, 2017, **29**, 1703463.

10 S. Zhu, L. Li, J. Liu, H. Wang, T. Wang, Y. Zhang, L. Zhang, R. S. Ruoff and F. Dong, *ACS Nano*, 2018, **12**, 1033-1042.

11 J. Wang, W. Guo, Z. Liu and Q. Zhang, *Adv. Energy Mater.*, 2023, **13**, 2300224.

12 L. Chen, F. Wang, Z. Tian, H. Guo, C. Cai, Q. Wu, H. Du, K. Liu, Z. Hao, S. He, G. Duan and S. Jiang, *Small*, 2022, **18**, 2201307.

13 L. Lyu, K.-d. Seong, J. M. Kim, W. Zhang, X. Jin, D. K. Kim, Y. Jeon, J. Kang and Y. Piao, *Nano-Micro Lett.*, 2019, **11**, 88.

14 J. Qian, H. Jin, B. Chen, M. Lin, W. Lu, W. M. Tang, W. Xiong, L. W. H. Chan, S. P. Lau and J. Yuan, *Angew. Chem. Int. Ed.*, 2015, **54**, 6800-6803.

15 H. Wang, C. Xu, Y. Chen and Y. Wang, *Energy Storage Mater.*, 2017, **8**, 127-133.

16 Z. Pan, M. Liu, J. Yang, Y. Qiu, W. Li, Y. Xu, X. Zhang and Y. Zhang, *Adv. Funct. Mater.*, 2017, **27**, 1701122.

17 C. Chen, Y. Zhang, Y. Li, J. Dai, J. Song, Y. Yao, Y. Gong, I. Kierzewski, J. Xie and L. Hu, *Energy Environ. Sci.*, 2017, **10**, 538-545.

18 Y. Liu, Z. Zeng, B. Bloom, D. H. Waldeck and J. Wei, *Small*, 2017, **14**, 1703237.

19 Z.-H. Huang, Y. Song, D.-Y. Feng, Z. Sun, X. Sun and X.-X. Liu, *ACS Nano*, 2018, **12**, 3557-3567.

20 B. Brown, I. A. Cordova, C. B. Parker, B. R. Stoner and J. T. Glass, *Chem. Mater.*, 2015, **27**, 2430-2438.

21 C. Xu, Z. Li, C. Yang, P. Zou, B. Xie, Z. Lin, Z. Zhang, B. Li, F. Kang and C. P. Wong, *Adv. Mater.*, 2016, **28**, 4105-4110.

22 H. Xu, X. Hu, H. Yang, Y. Sun, C. Hu and Y. Huang, *Adv. Energy Mater.*, 2015, **5**, 1401882.

23 K. S. Kumar, D. Pandey and J. Thomas, *ACS Energy Lett*., 2021, **6**, 3590-3599.

24 T. Zhai, S. Xie, M. Yu, P. Fang, C. Liang, X. Lu and Y. Tong, *Nano Energy*, 2014, **8**, 255-263.

25 Y. Song, T. Liu, B. Yao, M. Li, T. Kou, Z.-H. Huang, D.-Y. Feng, F. Wang, Y. Tong, X.-X. Liu and Y. Li, *ACS Energy Lett*., 2017, **2**, 1752-1759.

26 J. Shang, Q. Huang, L. Wang, Y. Yang, P. Li and Z. Zheng, *Adv. Mater.*, 2019, **32**, 1907088.

27 J.-C. Liu, H. Li, M. Batmunkh, X. Xiao, Y. Sun, Q. Zhao, X. Liu, Z.-H. Huang and T.-Y. Ma, *J. Mater. Chem. A*, 2019, **7**, 23941-23948.

28 T. Gao, Z. Zhou, J. Yu, J. Zhao, G. Wang, D. Cao, B. Ding and Y. Li, *Adv. Energy Mater.*, 2018, **9**, 1802578.

29 J. Li, L. An, H. Li, J. Sun, C. Shuck, X. Wang, Y. Shao, Y. Li, Q. Zhang and H. Wang, *Nano Energy*, 2019, **63**, 103848.

30 K. Shen, J. Ding and S. Yang, *Adv. Energy Mater*., 2018, **8**, 1800408.

31 Y. Wang, X. Wang, X. Li, X. Li, Y. Liu, Y. Bai, H. Xiao and G. Yuan, *Adv. Funct. Mater.*, 2020, **31**, 2008185.

32 M. Liu, Z. Cong, X. Pu, W. Guo, T. Liu, M. Li, Y. Zhang, W. Hu and Z. L. Wang, *Adv. Funct. Mater.*, 2019, **29**, 1806298.

33 L. Li, J. Zhang, Z. Peng, Y. Li, C. Gao, Y. Ji, R. Ye, N. D. Kim, Q. Zhong, Y. Yang, H. Fei, G. Ruan and J. M. Tour, *Adv. Mater*., 2016, **28**, 838-845.

34 C. Shen, X. Wang, S. Li, J. Wang, W. Zhang and F. Kang, *J. Power Sources*, 2013, **234**, 302-309.

35 Q. Zhang, J. Zhang, Z. Zhou, L. Wei and Y. Yao, *J. Mater. Chem. A*, 2018, **6**, 20145-20151.

36 J. Gao, C. Shao, S. Shao, F. Wan, C. Gao, Y. Zhao, L. Jiang and L. Qu, *Small*, 2018, **14**, e1801809.

37 H. Liu, K.-s. Moon, J. Li, Y. Xie, J. Liu, Z. Sun, L. Lu, Y. Tang and C.-P. Wong, *Nano Energy*, 2020, **77**, 105058.

38 X. Jin, L. Song, C. Dai, Y. Xiao, Y. Han, X. Zhang, X. Li, C. Bai, J. Zhang, Y. Zhao, Z. Zhang, L. Jiang and L. Qu, *Adv. Energy Mater.*, 2021, **11**, 2101523.

39 X. Pu, M. Liu, L. Li, S. Han, X. Li, C. Jiang, C. Du, J. Luo, W. Hu and Z. L. Wang, *Adv. Energy Mater.*, 2016, **6**, 1601254.

40 H. Wu, W. Zhang, S. Kandambeth, O. Shekhah, M. Eddaoudi and H. N. Alshareef, *Adv. Energy Mater.*, 2019, **9**, 1900482.

41 W. Song, J. Zhu, B. Gan, S. Zhao, H. Wang, C. Li and J. Wang, *Small*, 2017, **14**, 1702249.

42 Y. He, P. Zhang, M. Wang, F. Wang, D. Tan, Y. Li, X. Zhuang, F. Zhang and X. Feng, *Mater. Horiz.*, 2019, **6**, 1041-1049.

43 J. Qin, S. Wang, F. Zhou, P. Das, S. Zheng, C. Sun, X. Bao and Z.-S. Wu, *Energy Storage Mater.*, 2019, **18**, 397-404.

44 M. Wang, H. Shi, P. Zhang, Z. Liao, M. Wang, H. Zhong, F. Schwotzer, A. S. Nia, E. Zschech, S. Zhou, S. Kaskel, R. Dong and X. Feng, *Adv. Funct. Mater.*, 2020, **30**, 2002664.

45 H. Xiao, Z.-S. Wu, F. Zhou, S. Zheng, D. Sui, Y. Chen and X. Bao, *Energy Storage Mater.*, 2018, **13**, 233-240.

46 P. Zhang, Y. Li, G. Wang, F. Wang, S. Yang, F. Zhu, X. Zhuang, O. G. Schmidt and X. Feng, *Adv. Mater.*, 2019, **31**, e1806005.

47 W. Yang, Y. Zhu, Z. Jia, L. He, L. Xu, J. Meng, M. Tahir, Z. Zhou, X. Wang and L. Mai, *Adv. Energy Mater.*, 2020, **10**, 2001873.

48 J. Yun, Y. Lim, H. Lee, G. Lee, H. Park, S. Y. Hong, S. W. Jin, Y. H. Lee, S.-S. Lee and J. S. Ha, *Adv. Funct. Mater.*, 2017, **27**, 1700135.

49 R. Guo, J. Chen, B. Yang, L. Liu, L. Su, B. Shen and X. Yan, *Adv. Funct. Mater.*,

2017, **27**, 1702394.

50 M. Qiu, P. Sun, G. Cui, Y. Tong and W. Mai, *ACS Nano*, 2019, **13**, 8246-8255.

51 G. Sun, H. Yang, G. Zhang, J. Gao, X. Jin, Y. Zhao, L. Jiang and L. Qu, *Energy Environ. Sci.*, 2018, **11**, 3367-3374.

52 K.-H. Lee, S.-W. Kim, M. Kim, D. B. Ahn, Y.-K. Hong, S.-H. Kim, J. S. Lee and S.-Y. Lee, *Adv. Energy Mater.*, 2023, **13**, 2204327.

53 X. Huang, J. Huang, D. Yang and P. Wu, *Adv. Sci.*, 2021, **8**, 2101664.

54 X. Li, H. Li, X. Fan, X. Shi and J. Liang, *Adv. Energy Mater.*, 2020, **10**, 1903794.

55 W. Yang, J. Yang, J. J. Byun, F. P. Moissinac, J. Xu, S. J. Haigh, M. Domingos, M. A. Bissett, R. A. W. Dryfe and S. Barg, *Adv. Mater.*, 2019, **31**, 1902725.

56 S. Xu, Y. Dall'Agnese, G. Wei, C. Zhang, Y. Gogotsi and W. Han, *Nano Energy*, 2018, **50**, 479-488.

57 Y. Liu, B. Zhang, Q. Xu, Y. Hou, S. Seyedin, S. Qin, G. G. Wallace, S. Beirne, J. M. Razal and J. Chen, *Adv. Funct. Mater.*, 2018, **28**, 1706592.

58 C. J. Zhang, M. P. Kremer, A. Seral-Ascaso, S.-H. Park, N. McEvoy, B. Anasori, Y. Gogotsi and V. Nicolosi, *Adv. Funct. Mater.*, 2018, **28**, 1705506.

59 F. Li, J. Qu, Y. Li, J. Wang, M. Zhu, L. Liu, J. Ge, S. Duan, T. Li, V. K. Bandari, M. Huang, F. Zhu and O. G. Schmidt, *Adv. Sci*., 2020, **7**, 2001561.

60 J.-Q. Xie, Y.-Q. Ji, J.-H. Kang, J.-L. Sheng, D.-S. Mao, X.-Z. Fu, R. Sun and C.-P. Wong, *Energy Environ. Sci.*, 2019, **12**, 194-205.

61 S. Li, Q. Shi, Y. Li, J. Yang, T. H. Chang, J. Jiang and P. Y. Chen, *Adv. Funct. Mater.*, 2020, **30**, 2003721.

62 S.-W. Kim, K.-N. Kang, J.-W. Min and J.-H. Jang, *Nano Energy*, 2018, **50**, 410-416.

63 C. Zhang, L. McKeon, M. P. Kremer, S.-H. Park, O. Ronan, A. Seral-Ascaso, S. Barwich, C. Ó. Coileáin, N. McEvoy, H. C. Nerl, B. Anasori, J. N. Coleman, Y. Gogotsi and V. Nicolosi, *Nat. Commun*., 2019, **10**, 1795.

64 Y. Lei, W. Zhao, Y. Zhu, U. Buttner, X. Dong and H. N. Alshareef, *ACS Nano*, 2022, **16**, 1974-1985.

65 Y. Wang, Y. Zhang, G. Wang, X. Shi, Y. Qiao, J. Liu, H. Liu, A. Ganesh and L.

Li, *Adv. Funct. Mater.*, 2020, **30**, 1907284.

66 Y. Shao, J.-H. Fu, Z. Cao, K. Song, R. Sun, Y. Wan, A. Shamim, L. Cavallo, Y. Han, R. B. Kaner and V. C. Tung, *ACS Nano*, 2020, **14**, 7308-7318.

67 Y. Zeng, X. Zhang, Y. Meng, M. Yu, J. Yi, Y. Wu, X. Lu and Y. Tong, *Adv. Mater.*, 2017, **29**, 1700274.

68 M. Li, Q. He, Z. Li, Q. Li, Y. Zhang, J. Meng, X. Liu, S. Li, B. Wu, L. Chen, Z. Liu, W. Luo, C. Han and L. Mai, *Adv. Energy Mater.*, 2019, **9**, 1901469.

69 D. Wang, L. Wang, G. Liang, H. Li, Z. Liu, Z. Tang, J. Liang and C. Zhi, *ACS Nano*, 2019, **13**, 10643-10652.

70 Y. Zhang, S. Deng, Y. Li, B. Liu, G. Pan, Q. Liu, X. Wang, X. Xia and J. Tu, *Energy Storage Mater.*, 2020, **29**, 52-59.

71 Y. Jiang, D. Ba, Y. Li and J. Liu, *Adv. Sci.*, 2020, **7**, 1902795.

72 Y. Wu, M. Wang, Y. Tao, K. Zhang, M. Cai, Y. Ding, X. Liu, T. Hayat, A. Alsaedi and S. Dai, *Adv. Funct. Mater.*, 2019, **30**, 1907120.

73 Q. Chen, J. Jin, Z. Kou, C. Liao, Z. Liu, L. Zhou, J. Wang and L. Mai, *Small*, 2020, **16**, 2000091.